A conservative scheme for electromagnetic simulation of magnetized plasmas with kinetic electrons

J. Bao,[1,2] Z. Lin,[1,a)] and Z. X. Lu[2,3]

[1]*Department of Physics and Astronomy, University of California, Irvine, California 92697, USA*
[2]*Fusion Simulation Center, Peking University, Beijing 100871, People's Republic of China*
[3]*Max Planck Institut für Plasmaphysik, 85748 Garching, Germany*

A conservative scheme has been formulated and verified for gyrokinetic particle simulations of electromagnetic waves and instabilities in magnetized plasmas. An electron continuity equation derived from the drift kinetic equation is used to time advance the electron density perturbation by using the perturbed mechanical flow calculated from the parallel vector potential, and the parallel vector potential is solved by using the perturbed canonical flow from the perturbed distribution function. In gyrokinetic particle simulations using this new scheme, the shear Alfvén wave dispersion relation in the shearless slab and continuum damping in the sheared cylinder have been recovered. The new scheme overcomes the stringent requirement in the conventional perturbative simulation method that perpendicular grid size needs to be as small as electron collisionless skin depth even for the long wavelength Alfvén waves. The new scheme also avoids the problem in the conventional method that an unphysically large parallel electric field arises due to the inconsistency between electrostatic potential calculated from the perturbed density and vector potential calculated from the perturbed canonical flow. Finally, the gyrokinetic particle simulations of the Alfvén waves in sheared cylinder have superior numerical properties compared with the fluid simulations, which suffer from numerical difficulties associated with singular mode structures. *Published by AIP Publishing.* https://doi.org/10.1063/1.5016432

I. INTRODUCTION

The kinetic effects of electrons are important to long wavelength magnetohydrodynamic (MHD) instabilities and short wavelength drift-Alfvénic instabilities responsible for turbulence transport in magnetized plasmas, since the non-adiabatic electron can interact with, modify, and drive the low frequency instabilities.[1,2] Electromagnetic simulation with kinetic electrons encounters great computational challenges, especially for the long wavelength modes in high β plasmas (β is the ratio between kinetic and magnetic pressures),[3,4] which have been widely studied during the past two decades. In particular, the electromagnetic gyrokinetic particle simulation directly solving the electron drift kinetic equation cannot address efficiently the long wavelength modes, and the numerical performance becomes worse in high β plasmas. Early studies suggest that the perpendicular grid size should resolve electron skin depth for conventional perturbative (δf) simulations of shear Alfvén waves,[4] which represents a huge computational cost for the global simulation. The origin of this problem is that the large two adiabatic terms on both sides of the parallel Ampere's law using the canonical momentum $p_\parallel$ formulation cannot cancel with each other exactly when the grid size is larger than the electron skin depth in the conventional δf simulation,[5,6] which is sometimes referred to as the "cancellation problem" that affects the accuracy of the small non-adiabatic part.[7,8] Although many methods have been developed to overcome or avoid the "cancellation problem,"[5–15] electromagnetic gyrokinetic particle simulation with kinetic electrons is still computationally challenging.

In this work, we have formulated and verified a new conservative scheme using both the electron continuity equation and drift kinetic equation for gyrokinetic simulation of electromagnetic modes including long wavelength shear Alfvén waves. To demonstrate the successful application of the conservative scheme, we focus on the $p_\parallel$ formulation which suffers a severe numerical problem in early numerical studies.[3,4] In the conventional δf algorithm, it is found that the electron perturbed density and canonical flow measured from kinetic markers do not satisfy the electron continuity equation. Consequently, the electrostatic potential calculated from the density and the parallel vector potential calculated from the canonical flow are not consistent with each other, which results in an unphysically large parallel electric field. In the new conservative scheme, we use the electron continuity equation to time advance the electron density perturbation using the perturbed mechanical flow calculated from the parallel vector potential, and the parallel vector potential is solved by using the perturbed canonical flow from the kinetic markers. Using this new scheme in gyrokinetic particle simulation, we have verified the dispersion relation of the shear Alfvén wave in the shearless magnetic field, and Alfvén continuum damping and kinetic Alfvén wave propagation in the sheared magnetic field. This new conservative scheme has no restriction of the perpendicular grid size to resolve the electron skin depth for the long wavelength MHD wave simulation, and only requires a very small number of kinetic

a)Author to whom correspondence should be addressed: zhihongl@uci.edu

markers (20 markers per cell) to achieve sufficient accuracy in linear simulation. In addition to the simulations of the low frequency drift-Alfvénic modes described in the paper, the new conservative scheme has also been successfully applied to the simulations of radio frequency (RF) waves such as lower hybrid wave in tokamak plasmas.[16,17] Both simulation and theory have shown that an unphysically large $\delta E_\parallel$ is produced due to the inconsistency of the perturbed density and canonical flow in the simulation of the long wavelength shear Alfvén wave in the conventional δf scheme, which leads to the well-known numerical difficulties. In contrast, the conservative scheme guarantees the correctness of $\delta E_\parallel$ by enforcing the consistency between the perturbed density and canonical flow, and thus enforcing the consistency between the electrostatic potential and the parallel vector potential. Finally, by comparing the gyrokinetic particle simulation and fluid simulation of the kinetic Alfvén wave propagation in the sheared plasmas, we found that the fluid simulation suffers the artificial singular mode structure problem due to the model limitation, while gyrokinetic particle simulation physically avoids the artificial singularity by inducing the kinetic effects, i.e., electron Landau damping, which shows the superiority of our gyrokinetic particle simulation model.

The paper is organized as follows: the physics model of the conservative scheme for electromagnetic simulations with drift kinetic electrons is introduced in Sec. II. The simulation results of shear Alfvén waves in both the uniform and sheared magnetic field are shown in Sec. III. In Sec. IV, the effects of particle noise in the PIC simulations of long wavelength shear Alfvén waves are studied theoretically for the conventional perturbative scheme and conservative scheme. Section V is the conclusion.

II. CONSERVATIVE SCHEME

Electromagnetic simulation with kinetic electrons suffers severely numerical instabilities when $\beta_e \gg m_e/m_i$ and $k_\perp^2 d_e^2 \ll 1$ ($k_\perp$ is the perpendicular wave vector and d_e is the electron skin depth) in earlier gyrokinetic particle simulations.[3,4] In this work, we are able to avoid these numerical instabilities by using an electron continuity equation to ensure the density conservation in the simulation, which is referred to as the conservative scheme. The ordering adopted in the paper is

$$\frac{\omega}{\Omega_i} \sim \frac{\delta f}{f} \sim \frac{e\phi}{T} \sim \frac{\delta B}{B_0} \sim \frac{k_\parallel}{k_\perp} \sim \frac{1}{k_\perp L} \sim O(\varepsilon) \ll 1,$$

where ω and $\Omega_i = eB_0/cm_i$ are the physical mode frequency and ion cyclotron frequency, δf and f are the perturbed and total particle distributions, ϕ and δB are the perturbed electrostatic potential and perturbed magnetic field, and $k_\perp$ and $k_\parallel$ are the perpendicular and parallel wave vectors. L is plasma equilibrium scale length $L^{-1} \sim (L_n^{-1} = \nabla \ln n, L_T^{-1} = \nabla \ln T, L_B^{-1} = \nabla \ln B_0)$ (T is plasma temperature, n is plasma density, and B_0 is equilibrium magnetic field).

The electron drift kinetic equation uses guiding center position $\mathbf{R}$, parallel canonical momentum $p_\parallel = m_e v_\parallel$

$+ q_e \delta A_\parallel / c$ (m_e and q_e denote electron mass and charge, respectively), and magnetic momentum μ as independent variables in five dimensional phase space[18,19]

$$\frac{\partial}{\partial t}\left(f_e B_\parallel^*\right) + \nabla \cdot \left(\dot{\mathbf{R}} f_e B_\parallel^*\right) + \frac{\partial}{\partial p_\parallel}\left(\dot{p}_\parallel f_e B_\parallel^*\right) = 0, \quad (1)$$

$$\dot{\mathbf{R}} = \frac{1}{m_e}\left(p_\parallel - \frac{q_e}{c}\delta A_\parallel\right)\frac{\mathbf{B}_0^*}{B_\parallel^*} + \frac{c\mathbf{b}_0}{q_e B_\parallel^*}$$
$$\times (\mu\nabla B_0 + q_e\nabla\Psi_l + q_e\nabla\Psi_{nl}), \quad (2)$$

$$\dot{p}_\parallel = -\frac{\mathbf{B}_0^*}{B_\parallel^*}\cdot(\mu\nabla B_0 + q_e\nabla\Psi_l + q_e\nabla\Psi_{nl}), \quad (3)$$

where $f_e = f_e(\mathbf{R}, p_\parallel, \mu, t)$ is the electron guiding center distribution, $\mathbf{B}_0 = B_0\mathbf{b}_0$ is the equilibrium magnetic field, $\mathbf{B}_0^* = \mathbf{B}_0 + \frac{c}{q_e}p_\parallel\nabla\times\mathbf{b}_0$, $B_\parallel^* = \mathbf{b}_0\cdot\mathbf{B}_0^*$, ϕ is the electrostatic potential, $\delta A_\parallel$ is the vector potential, and $\Psi_l = \phi - \frac{p_\parallel\delta A_\parallel}{m_e c}$ and $\Psi_{nl} = \frac{q_e\delta A_\parallel^2}{2m_e c^2}$ are the linear and nonlinear parts of the generalized potential, respectively. Equations (1)–(3) are also referred to as $p_\parallel$ formulation in a conservative form and satisfy the Liouville's theorem.[19]

In order to minimize the particle noise, the perturbative (δf) method[20,21] is widely used in particle-in-cell simulations. In the perturbative (δf) method, the distribution function f_e is decomposed into equilibrium and perturbed parts as $f_e = f_{e0} + \delta f_e$. In the lowest order equilibrium part, Eq. (1) reduces to

$$L_0 f_{e0} = 0, \quad (4)$$

where $L_0 = \frac{\partial}{\partial t} + \left(\frac{p_\parallel}{m_e B_\parallel^*}\mathbf{B}_0^* + \frac{c\mu}{q_e B_\parallel^*}\mathbf{b}_0\times\nabla B_0\right)\cdot\nabla - \frac{\mu}{B_\parallel^*}\mathbf{B}_0^*$
$\cdot\nabla B_0\frac{\partial}{\partial p_\parallel}$ is the equilibrium propagator. The equilibrium solution f_{e0} can be approximated as a Maxwellian: $f_{e0} = n_{e0}\left(\frac{m_e}{2\pi T_{e0}}\right)^{3/2}\exp\left(-\frac{p_\parallel^2/m_e + 2\mu B}{2T_{e0}}\right)$ when the neoclassical effects are not important.

Subtracting Eq. (1) by Eq. (4), the equation for the perturbed distribution δf_e is

$$L\delta f_e = -(\delta L_1 + \delta L_2)f_{e0}, \quad (5)$$

where $L = \frac{\partial}{\partial t} + \dot{\mathbf{R}}\cdot\nabla + \dot{p}_\parallel\frac{\partial}{\partial p_\parallel}$ is the total propagator, and the perturbed propagator $\delta L = \delta L^L + \delta L^{NL}$ consists of linear and nonlinear parts

$$\delta L^L = \left(-\frac{q_e\delta A_\parallel}{cm_e}\frac{\mathbf{B}_0^*}{B_\parallel^*} + \frac{c\mathbf{b}_0\times\nabla\Psi_l}{B_\parallel^*}\right)\cdot\nabla - q_e\frac{\mathbf{B}_0^*}{B_\parallel^*}\cdot\nabla\Psi_l\frac{\partial}{\partial p_\parallel}$$

$$\delta L^{NL} = \frac{c\mathbf{b}_0}{q_e B_\parallel^*}\times q_e\nabla\Psi_{nl}\cdot\nabla - q_e\frac{\mathbf{B}_0^*}{B_\parallel^*}\cdot\nabla\Psi_{nl}\frac{\partial}{\partial p_\parallel}.$$

Defining the particle weight as $w_e = \delta f_e/f_e$, the weight equation can be derived by using Eq. (5)

$$\frac{dw_e}{dt} = Lw_e = -(1 - w_e)\frac{1}{f_{e0}}(\delta L_1 + \delta L_2)f_{e0}. \quad (6)$$

The parallel scalar potential $\delta A_\parallel$ is solved from Ampere's law

$$\left(\nabla_\perp^2 - \frac{\omega_{pe}^2}{c^2} - \frac{\omega_{pi}^2}{c^2}\right)\delta A_\parallel = \frac{4\pi}{c}\left(en_{e0}U_{\parallel ec} - Z_i n_{i0}U_{\parallel ic}\right), \quad (7)$$

where $U_{\parallel ec}$ and $U_{\parallel ic}$ are the parallel canonical flow calculated from the kinetic markers

$$U_{\parallel\alpha c} = \frac{1}{n_{\alpha 0}m_\alpha}\int \mathbf{dv}p_\parallel\delta f_\alpha, \quad (8)$$

where $\alpha = i, e$ and $\int \mathbf{dv} = (2\pi B_0/m_\alpha^2)\int dp_\parallel d\mu$. The appearances of the second and third terms on the LHS of Eq. (7) are due to the adiabatic parts associated with $\delta A_\parallel$ from particle canonical momentum $p_\parallel$. The last terms on both sides of Eq. (7) associated with ions are dropped in this paper for simplicity.

Integrating Eq. (5) in velocity space and keeping terms up to the $O(\varepsilon^2)$ order, we can derive the electron continuity equation in a conservative form

$$\frac{\partial\delta n_e}{\partial t} + \nabla\cdot\left[n_{e0}\left(\delta u_{\parallel e}\mathbf{b_0} + \mathbf{V_E} + u_{\parallel e0}\frac{\delta\mathbf{B}}{B_0}\right)\right.$$
$$\left. + \frac{1}{T_{e0}}\left(\delta P_{\perp e}\mathbf{V_g} + \delta P_{\parallel e}\mathbf{V_c}\right) + \frac{n_{e0}\delta u_{\parallel e}}{B_0}\delta\mathbf{B} + \delta n_e\mathbf{V_E}\right] = 0,$$
$$(9)$$

where $\mathbf{V_E} = c\mathbf{b_0}\times\nabla\phi/B_0$, $\mathbf{V_c} = \frac{cT_0}{q_e B_0}\mathbf{b_0}\times(\mathbf{b_0}\cdot\nabla\mathbf{b_0})$, and $\mathbf{V_g} = \frac{cT_0}{q_e B_0^2}\mathbf{b_0}\times\nabla B_0$. $u_{\parallel e0} = -\frac{c}{4\pi e n_{e0}}\mathbf{b_0}\cdot\nabla\times\mathbf{B_0}$ is approximated as the equilibrium current, $\delta P_{\parallel e} = \frac{1}{m_e}\int \mathbf{dv}p_\parallel^2\delta f_e$, $\delta P_{\perp e} = \int \mathbf{dv}\mu B_0\delta f_e$, and $\delta\mathbf{B} = \nabla\times(\delta A_\parallel\mathbf{b_0})$ is the magnetic perturbation. $\delta u_{\parallel e} = U_{\parallel ec} - \frac{q_e\delta A_\parallel}{cm_e}$ represents the mechanical flow in Eq. (9). However, due to the fact that $|U_{\parallel ec}| \approx |\frac{q_e\delta A_\parallel}{cm_e}| \gg |\delta u_{\parallel e}|$ in $\beta_e \gg m_e/m_i$ and $k_\perp^2 d_e^2 \ll 1$ regimes, it will bring severe "cancellation problem" when we calculate $\delta u_{\parallel e}$ by using $\delta u_{\parallel e} = U_{\parallel ec} - \frac{q_e\delta A_\parallel}{cm_e}$ with particle noise. In order to overcome this problem, we calculate $\delta u_{\parallel e}$ by inverting the original Ampere's law as

$$n_{e0}e\delta u_{\parallel e} = \frac{c}{4\pi}\nabla_\perp^2\delta A_\parallel, \quad (10)$$

where $\delta A_\parallel$ is solved from Eq. (7), and the ion current is dropped for simplicity. To the leading order terms up to $O(\varepsilon^2)$, Eq. (9) integrated from the drift kinetic equation in the $p_\parallel$ formulation is the same with the $v_\parallel$ formulation ones: Eq. (28) in Deng et al.[22] and Eq. (21) in Bao et al.[33]

The Poisson's equation is[23]

$$\frac{4\pi Z_i^2 n_{i0}}{T_{i0}}\left(\phi - \tilde\phi\right) = 4\pi(Z_i\delta n_i - e\delta n_e), \quad (11)$$

where n_{i0} and T_{i0} are the ion equilibrium density and temperature, respectively. Z_i represents ion charge, and $\delta n_i = \int \mathbf{dv}\delta f_i$ is ion perturbed density. The terms on the left hand side of Eq. (11) represent ion polarization density.

Equations (1)–(3) and (6)–(11) form a closed system together with the ion gyrokinetic equation and represent the new conservative scheme, which can be applied to the nonlinear toroidal electromagnetic simulations with kinetic electrons. Note that by using the canonical momentum as an independence phase space coordinate, we avoid the well-

known numerical issues of explicit time derivative of the vector potential to calculate the inductive parallel electric field. In this paper, we focus on verifying this new model for the linear shear Alfvén wave simulation in both the shearless and sheared magnetic field. The application to the nonlinear and toroidal simulations will be reported in the future.

If we neglect ion finite Larmor radius (FLR) effects and parallel motion, then ion $\mathbf{E}\times\mathbf{B}$ drift cancels out with electron $\mathbf{E}\times\mathbf{B}$ drift, and ion only contributes to the polarization density [appears on the left hand side of Eq. (11)]. The linear dispersion relation in the uniform plasmas can be derived as

$$\left(\frac{\omega^2}{k_\parallel^2 V_A^2} - 1\right)[1 + \xi_e Z(\xi_e)] = k_\perp^2\rho_s^2, \quad (12)$$

where $\xi_e = \omega/\sqrt{2}k_\parallel v_{the}$, $\rho_s = C_s/\Omega_{ci}$, $v_{the} = \sqrt{T_{e0}/m_e}$, $C_s = \sqrt{T_{e0}/m_i}$, $V_A = B_0/\sqrt{4\pi n_{i0}m_i}$ and $Z(\xi_e)$ is the plasma dispersion function

$$Z(\xi_e) = \frac{1}{\sqrt{\pi}}\int_{-\infty}^{+\infty}\frac{e^{-t^2}}{t - \xi_e}dt.$$

Thus, compared to the dispersion relation derived from the Lin-Chen fluid-kinetic hybrid electron model,[6] the ion acoustic wave is artificially removed in this paper for simplicity, but can easily be incorporated by retaining the kinetic ion contribution.

III. SIMULATION RESULTS

A. Shear-less magnetic field

To verify the new conservative scheme, we implement it in a 2D slab code to simulation the kinetic shear Alfvén wave (KAW) in a uniform magnetic field pointing in the positive z-direction. The KAW wave vector is in the x-z plane. The electrons are treated using the drift kinetic equation and the ions as the fixed background with only contribution to the polarization density. We first carry out simulations with $T_{e0} = 5.0\,\text{keV}$, $B = 1.5\,\text{T}$, $n_{e0} = 1\times 10^{13}\,\text{cm}^{-3}$, $\beta_e = 0.9\%$, and $k_\parallel/k_\perp = 0.01$, and verify the wavelength $k\rho_s$ dependence of frequency as well as $\Delta x/d_e$ (Δx is the perpendicular grid size and d_e is the electron skin depth) dependence. We change the wavelength in the range of $0.01 < k\rho_s < 0.48$. The grid numbers per wavelength in the parallel and perpendicular directions are fixed as $N_z = 64$ and $N_x = 60$, thus the grid size also changes with the wavelength. We use 20 markers per cell in all simulations of this paper. We give an initial density perturbation, and then let the perturbation evolve self-consistently. The KAW frequencies measured from simulations using the electron continuity equation agree with the theory well for both short and long wavelengths regimes. Most importantly, the perpendicular grid size can be much larger than the electron skin depth in the long wavelength regime as shown in Fig. 1. This shows that the perpendicular grid size is not restricted by the electron skin depth when we calculate the density perturbation from the electron continuity equation. For comparison, the simulation results deviate from the theoretical predication in the regime $k\rho_s \ll 1$ or $\Delta x/d_e \gg 1$ when we calculate the density
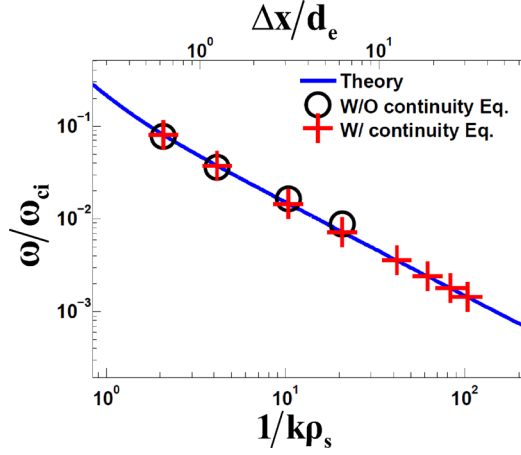
FIG. 1. Dependence of KAW frequency on wavelength (bottom) and perpendicular grid size (top). The red crosses represent results from the new conservative scheme with the continuity equation, and the black circles represent results from the conventional δf scheme without the continuity equation.

perturbation from kinetic markers directly, which are shown by the black circles in Fig. 1. In these cases, without applying the electron continuity equation, the high frequency noise level greatly increases for the longer wavelength regime, which makes it difficult to measure the frequency when $k\rho_s < 0.05$. The numerical convergence tests with respect to particle number per cell N_P, time step $k_{\parallel}v_{the}\Delta t$, perpendicular grid number per wavelength N_x, and parallel grid number per wavelength N_z are shown in Fig. 2 for the $k_{\perp}\rho_s = 0.048$ case.

Next, we apply an antenna with the theoretical frequency to excite the Alfvén waves in different wavelength regimes: $1/k\rho_s = 4.2(\Delta x/d_e = 1.2)$, $1/k\rho_s = 20.8(\Delta x/d_e = 6.2)$, and $1/k\rho_s = 41.5(\Delta x/d_e = 12.5)$, respectively. The upper panels of Figs. 3(a)–3(c) give the time histories of the electrostatic
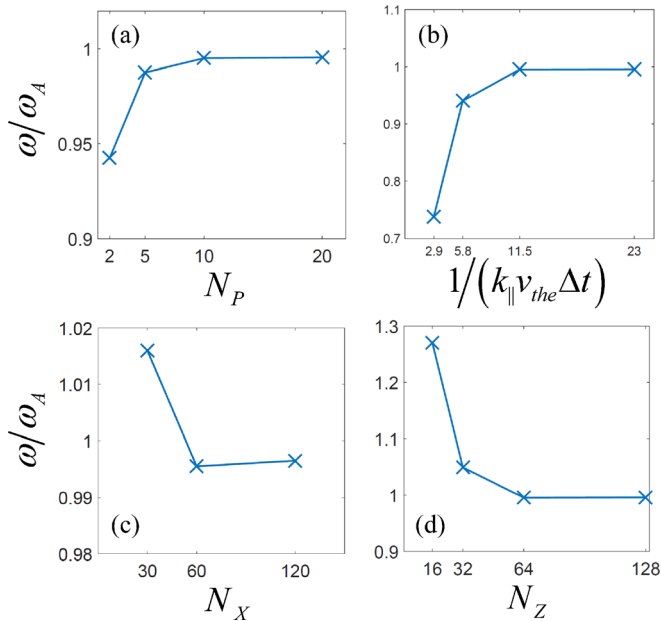

FIG. 2. Numerical convergences with respect to (a) particle number per cell N_P, (b) time step $k_{\parallel}v_{the}\Delta t$, (c) perpendicular grid number per wavelength N_x, and (d) parallel grid number per wavelength N_z. Simulations were performed with $k_{\perp}\rho_s = 0.048$ and $\beta_e = 0.9\%$. Frequency ω is normalized by $\omega_A = k_{\parallel}V_A\sqrt{1 + k_{\perp}^2\rho_s^2}$.

potential ϕ at the position with the maximal value from the conventional scheme and conservative scheme. As the wavelength or perpendicular grid size increases, our simulation model does not suffer numerical noise or instability as shown by the blue lines. However, the noise level of the conventional δf scheme increases with the perpendicular grid size as shown by the red lines, even though the time step of the red lines is 10 times shorter than the blue lines in Fig. 3(c) for numerical stabilization. In the conservative scheme, simulations using the continuity equation, we plot in the lower panels of Figs. 3(a)–3(c), the perturbed densities calculated from the kinetic markers in order to compare with the results from the continuity equation. The discrepancy of the perturbed densities calculated from the kinetic markers and the continuity equation becomes larger as the wavelength or perpendicular grid size increases.

The reason for the inconsistency between the perturbed density and canonical flow calculated from the kinetic markers in the δf method can be interpreted as follows. The assumption of the equilibrium distribution function f_{e0} as the analytical Maxwellian $f_{Maxwellian}$ is not identical to the marker distribution f_{Marker} in the simulations due to particle noise, and the error between these two distributions $\Delta f = f_{Marker} - f_{Maxwellian}$ accumulates in the simulation through Eq. (6) for the particle weight. Thus, after integrating the perturbed density and canonical flow from the kinetic markers using the particle weight, the electron continuity equation is not satisfied due to this error.

For shear Alfvén waves in the long wavelength limit, the parallel electric field $\delta E_{\parallel}$ is nearly 0, which requires that the electrostatic electric field $\delta E_{\parallel}^e = -\mathbf{b_0} \cdot \nabla\phi$ and the inductive electric field $\delta E_{\parallel}^i = -(1/c)\partial\delta A_{\parallel}/\partial t$ evolve consistently and cancel with each other. Since we apply $p_{\parallel}$ formulation and $\delta E_{\parallel}^i$ does not appear explicitly in the simulation, here we calculated $\delta E_{\parallel}^i$ numerically from the output information of $\delta A_{\parallel}$ for diagnosis. In the conservative scheme, the consistency of $\delta E_{\parallel}^e$ and $\delta E_{\parallel}^i$ is enforced by using the continuity equation, and the total $\delta E_{\parallel}$ is much smaller than its electrostatic or inductive components as shown in Fig. 4(a). When we calculated the perturbed density from the kinetic markers, the inconsistency of $\delta E_{\parallel}^e$ and $\delta E_{\parallel}^i$ gives rise to an unphysically large $\delta E_{\parallel}$ as shown in Fig. 4(b). These observations prove our conclusion that the perturbed density and canonical flow calculated from the kinetic markers do not satisfy the continuity equation, and the corresponding electrostatic potential and vector potential do not evolve consistently in the conventional δf method, which causes the numerical instabilities in the electromagnetic simulation of the long wavelength modes in high β_e plasmas. Furthermore, the theoretical study of the error effects on the dispersion relation and the parallel electric field are given in Sec. IV, which confirms that the inconsistency of the perturbed density and canonical flow in the conventional δf scheme can cause significant deviations of the parallel electric field from the exact solution.

Second, we carry out simulations of shear Alfvén waves in different β_e regimes. In the simulations, $k\rho_s = 0.10$ and $k\rho_s = 0.48$ are chosen as long and short wavelengths cases, respectively. We increase the plasma density n_{e0} from 1×10^{13} cm^{-3} to 20.0×10^{13} cm^{-3} for different β_e values. Other parameters are the same with Fig. 1. The grid number per
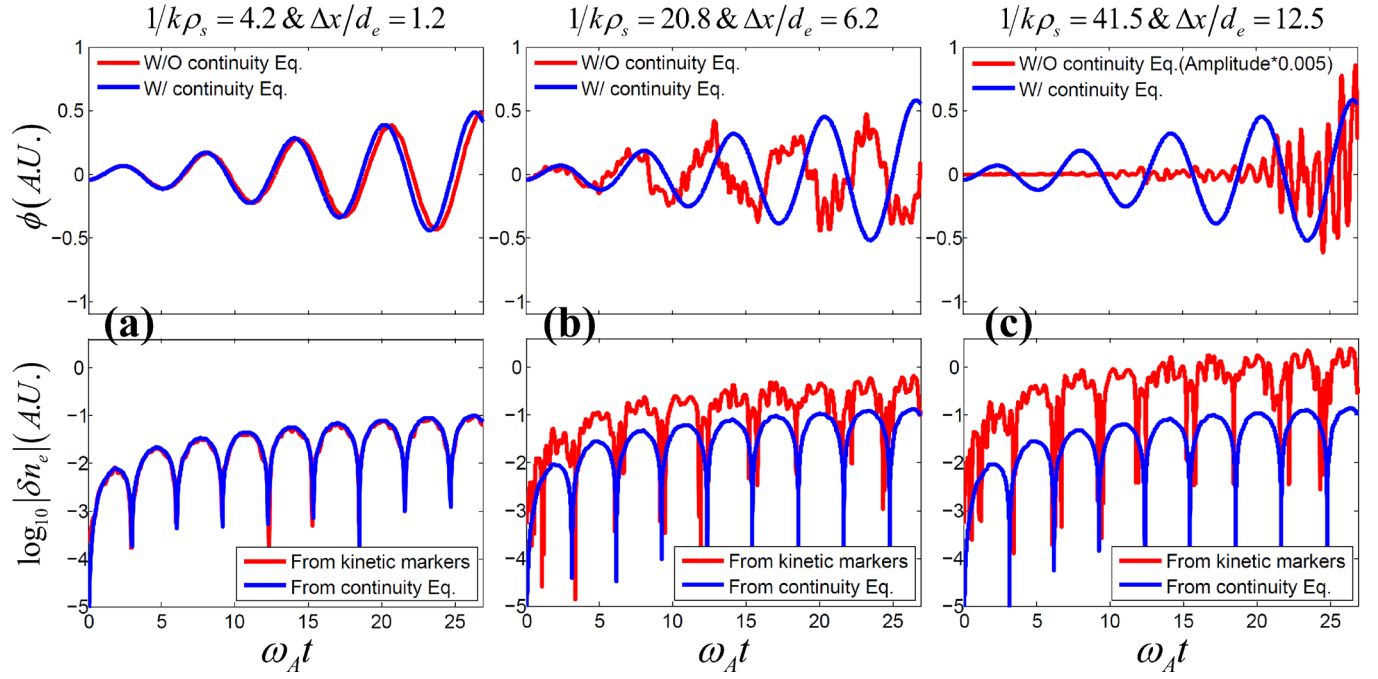
FIG. 3. Time histories of electrostatic potential (upper panels) and density perturbation (lower panels) for various wavelengths. In the upper panels, the red lines are from the conventional δf scheme and the blue lines are from the conservative scheme using the continuity equation. In the lower panels, both the red lines and blue lines represent density perturbation calculated from kinetic markers and from the continuity equation in the same simulation using the conservative scheme.

parallel wavelength N_z increases with β_e for numerical convergence, e.g., $N_z = 128$ is used for $\beta_e = 18\%$ simulation, while the grid number per perpendicular wavelength $N_x = 60$ is enough for the convergence of all the cases in Fig. 5. Using the conservative scheme, the frequencies and damping

rates measured from the simulations agree well with the theory for $\beta_e \gg m_e/m_i$, and the corresponding perpendicular grid size does not need to resolve the electron skin depth in the very high β_e cases. For the $k\rho_s = 0.10$ case, the damping rates of the shear Alfvén wave are too small to measure, which are absent in Fig. 5. Therefore, the accuracy of the dispersion relation of the shear Alfvén wave can be achieved by using the electron continuity equation in the high β_e ($\beta_e \gg m_e/m_i$) and long wavelength regimes without resolving the electron skin depth.

B. Sheared magnetic field

We now implement our model into the gyrokinetic toroidal code (GTC)[24] and carry out simulations of Alfvén wave in a cylinder plasma with magnetic shear. For comparisons with the kinetic simulations, we also suppress the kinetic effects in GTC to carry out fluid simulations of the Alfvén wave with the same parameters. In the fluid simulation, we apply the momentum equation by taking the first moment of the drift kinetic equation

$$\frac{\partial U_{\|ec}}{\partial t} + \frac{q_e}{m_e}\mathbf{b_0} \cdot \nabla\phi + \frac{B_0}{m_e n_{e0}}\mathbf{b_0} \cdot \nabla\left(\frac{\delta P_\|}{B_0}\right) = 0, \quad (13)$$

where the pressure $\delta P_\| = \delta n_e T_{e0}$ using isothermal assumption. Equations (7), (9)–(11) and (13) form a closed system for fluid simulation with finite electron mass and temperature, which is equivalent to the fluid model with electron inertia proposed by Liu and Chen.[25,26]

In inhomogeneous plasmas, both $k_\| = [nq(r) - m]/q(r)R$ and Alfvén speed V_A vary spatially with the equilibrium magnetic field and density, which gives rise to the continuum
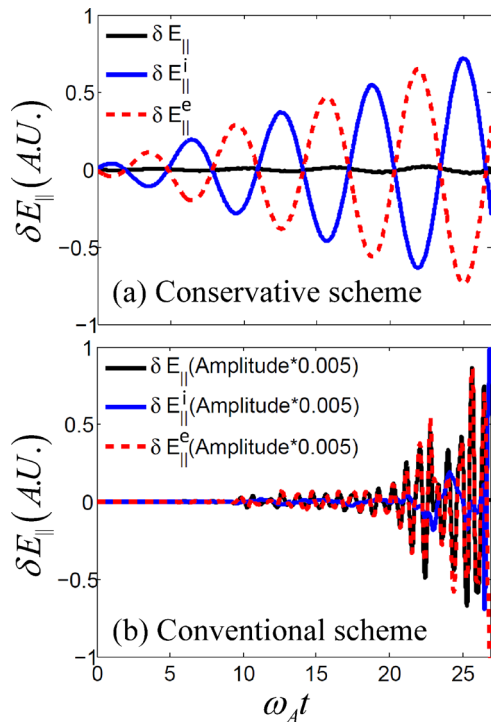

FIG. 4. The time histories of the parallel electric field $\delta E_\|$ for $1/k\rho_s = 41.5$, (a) is from the conservative scheme and (b) is from the conventional δf scheme.
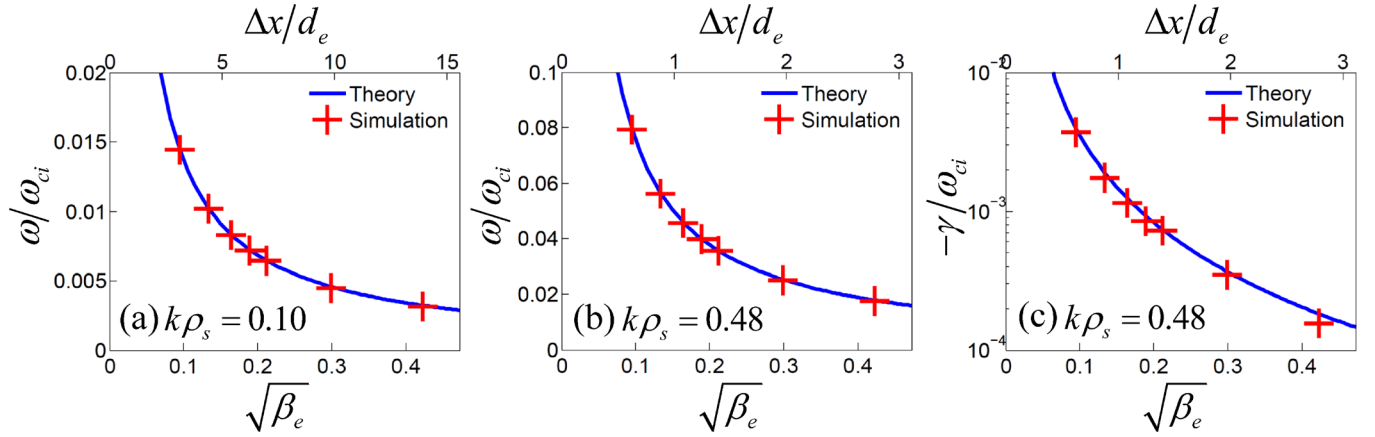
FIG. 5. Dependence of frequency on electron beta β_e and perpendicular grid size $\Delta x/d_e$ for (a) $k\rho_s = 0.10$ and (b) $k\rho_s = 0.48$. (c) dependence of damping rate on electron beta β_e and perpendicular grid size $\Delta x/d_e$ for $k\rho_s = 0.48$. The red crosses represent simulation results from the conservative scheme.

damping of the Alfvén waves. In our simulation, the magnetic field is $B_0 = 2.0$ T, equilibrium density and electron temperature are uniform with $n_{e0} = n_{i0} = 2.0 \times 10^{13}$ cm^{-3} and $T_{e0} = 5.0$ keV, the electron beta value is $\beta_e = 1.0\%$, the length of the cylinder is $l = 2\pi R_0 (R_0 = 1.0$ m$)$, the minor radius is $a = 0.5$ m (our simulation domain is from $r_{\min} = 0.39a$ to $r_{\max} = 0.86a$, and $a/\rho_s = 139$), and the safety factor q varies monotonously as $q = 0.76(r/a)^2 + 0.8$. The perpendicular grid size is $\Delta x/d_e = 2.0$ and the time step is $\Delta t = 0.04 R_0/v_{the}$. We apply an initial density perturbation with the poloidal mode number $m = 3$ ($k_\theta \rho_s = 0.034$ at $r = 0.63a$, and initial $k_r \rho_s = 0.048$) and axial mode number $n = 2$. The time history of the electrostatic potential ϕ at the radial position $r = 0.63a$ is shown by Fig. 6(a). The Alfvén wave damps more quickly in the simulation with drift kinetic electrons than fluid electrons. As predicted, the time dependence of the mode amplitude due to the continuum damping is proportional to $1/t$.[27–29] In order to verify the simulation with the theory, we compare the ϕ amplitude evolution between

fluid simulation and kinetic simulation in Fig. 6(b). It is found that the wave amplitude histories from both fluid (red line) and kinetic (blue line) simulations agree with the $1/t$ fitting (the black dashed line) at the initial phase, which verifies the Alfvén continuum damping. However, in the kinetic electron simulation, the electron Landau damping becomes the dominant damping mechanism later on, which is close to an exponential decay as shown by the black solid fitting line. For comparison, in the fluid simulation, the time history of ϕ agrees with the $1/t$ fitting, and the slight deviation in the later period is due to the finite electron mass and thermal pressure effects, which cause the propagation of Alfvén waves and affect the continuum damping. The radius-time plots of the absolute value of the electrostatic potential ϕ from kinetic and fluid simulations are shown by Figs. 6(c) and 6(d), respectively. Figure 6(d) shows that the continuum damping in the fluid simulation causes the increase of the radial wave vector, eventually leading to a singular radial structure (which is not physical). In contrast, the kinetic effects in the kinetic
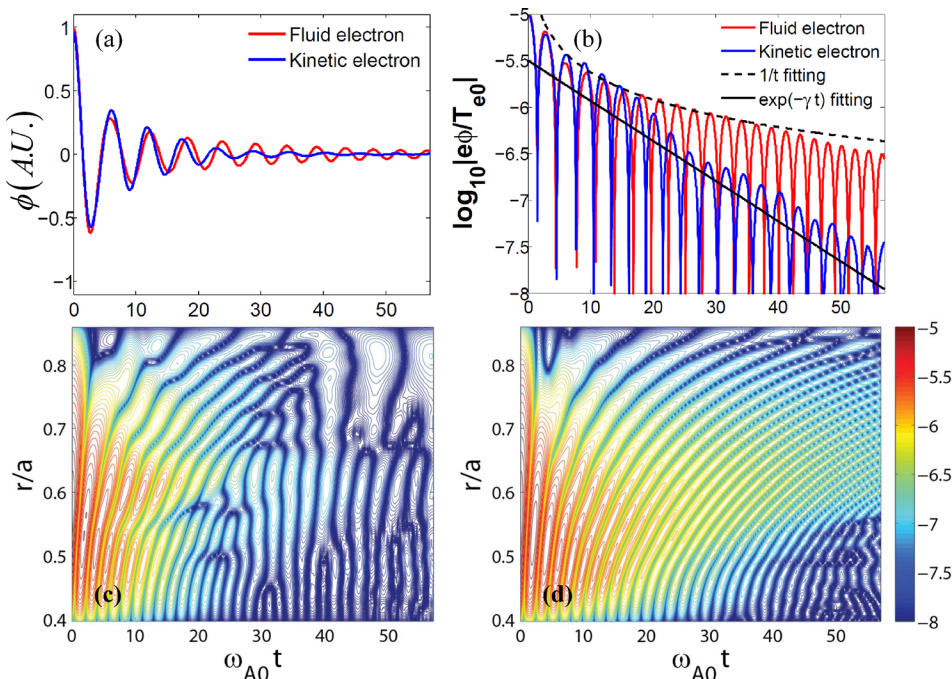

FIG. 6. (a) Time evolution of electrostatic potential ϕ at $r = 0.63a$ and (b) corresponding absolute value of electrostatic potential. (c) and (d) are radius-time plots of $\log_{10}(e|\phi|/T_{e0})$ from kinetic and fluid simulations, respectively.
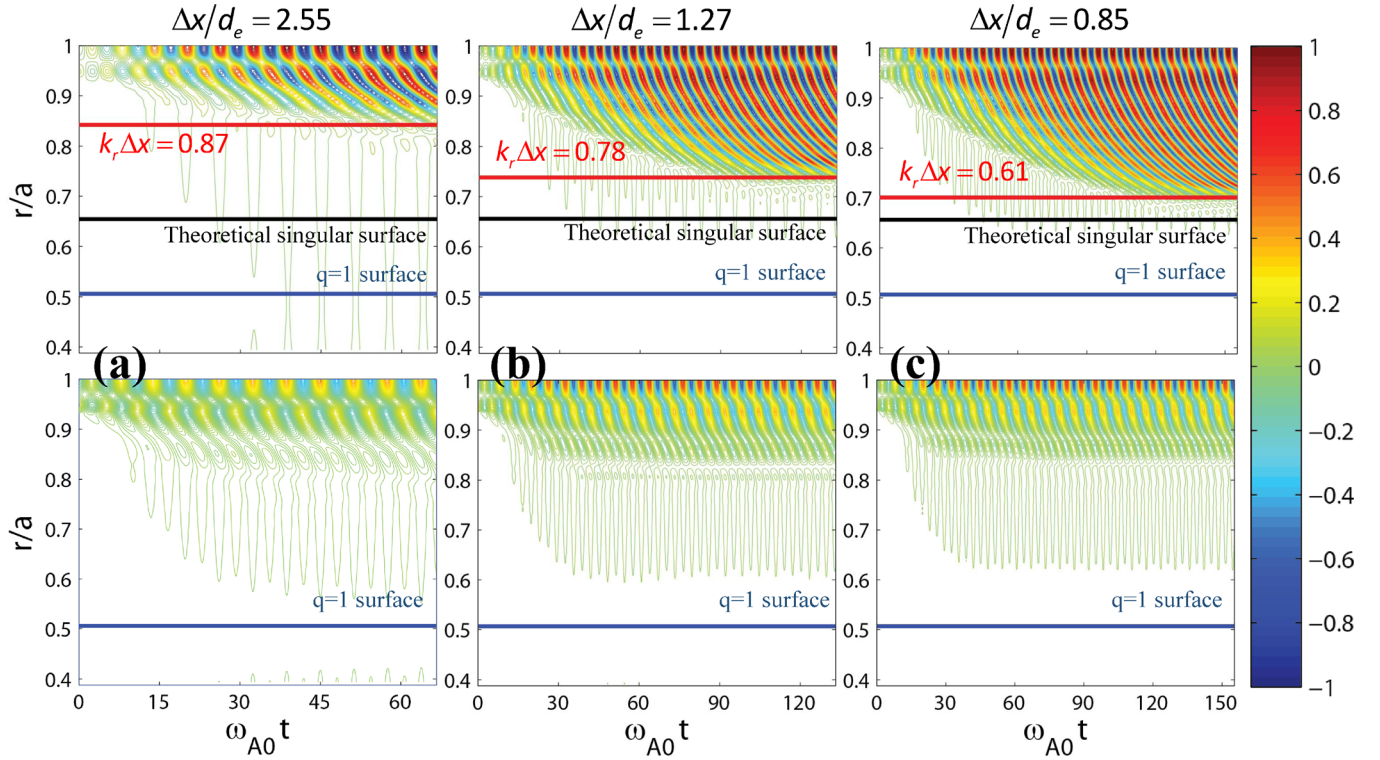
FIG. 7. Radius-time plots of radial electric field $\delta E_r (A.U.)$ of the shear Alfvén wave propagation using various perpendicular grid sizes. The upper panels are from fluid simulation and the lower panels are from kinetic simulation.

simulation result in the Landau damping and the formation of normal modes with discrete frequencies (which are more physical Landau eigen states) as shown in Fig. 6(c). This indicates that the kinetic approach for the simulations of Alfvén waves is not just more physical, but also numerically superior than the fluid approach.

Furthermore, we carry out simulations of KAW using antenna excitation to verify the propagation in cylinder plasmas. The radial simulation domain is from $r_{\min} = 0.39a$ to $r_{\max} = a$. The other parameters are the same as the continuum damping simulation earlier in this subsection. We excite the KAW with the poloidal mode number $m = 3$ ($k_\theta \rho_s = 0.022$ at $r = a$) and the axial mode number $n = 3$ at the edge by using an external antenna with local shear Alfvén frequency $\omega_{A0} = k_{\|0} V_A$, where $k_{\|0}$ is the parallel wave vector at $r = a$. The excited shear Alfvén wave can convert to the kinetic Alfvén wave at the launching position since it is also the resonant layer where the relation $\omega_{A0} = k_\|(a) V_A$ is satisfied; then, the KAW can propagate across the magnetic field lines.[30,31]

In Fig. 7, we present the radial electric field $\delta E_r = -\partial \phi / \partial r$ of the Alfvén wave propagation from fluid and kinetic simulations with different perpendicular grid sizes. In the fluid simulation, the dispersion relation of the shear Alfvén wave with finite electron mass is $k_\perp^2 = \frac{1}{\rho_s^2} (1 - \frac{\omega^2}{k_\|^2(r) V_A^2}) / (\frac{\omega^2}{k_\|^2(r) v_{the}^2} - 1)$, thus there exists the singular surface ($k_\perp^2 \to +\infty$), where $\omega_{A0} = k_\|(r) v_{the}$ is satisfied for the Alfvén wave propagation with a fixed frequency. For comparison, the dispersion relation of the shear Alfvén wave with zero electron inertial term is $k_\perp^2 = \frac{1}{\rho_s^2} (\frac{\omega^2}{k_\|^2(r) V_A^2} - 1)$, and

the singular surface for the shear Alfvén wave with $m = n = 3$ is $q = 1$ surface where $k_\|(r) = 0$. In the simulation, we use the finite electron mass model. From the upper panels of Figs. 7(a)–7(c), it can be seen that the perpendicular wave vector will increase as the Alfvén wave propagates toward the singular surface. The singular surface in the simulation deviates from the theoretical predictions, which is due to the fact that the spatial resolution is not enough to resolve the short radial wavelength. The shear Alfvén wave propagates to the theoretical singular surface only when the perpendicular grid size $\Delta x \to 0$. For comparison, there is no singularity in the drift kinetic electron simulation as shown by the lower panels of Figs. 7(a)–7(c). The perpendicular grid size is less important, since the kinetic effects lead to the formation of a normal mode and thus prevent the increase of the perpendicular wave vector. This also shows the necessity of the kinetic approach for the simulations of Alfvén waves as illustrated in the earlier study of continuum damping in this subsection.

IV. ERROR ESTIMATIONS

A. Error effects on the dispersion relation

We have demonstrated in Sec. III that the perpendicular grid size should resolve the electron skin depth for the conventional δf scheme in order to control the error level, while there is no restriction of the perpendicular grid size in the conservative scheme. In this part, we derive the dispersion relation of the shear Alfvén wave with the particle noise effect for the conventional δf scheme and the conservative scheme (continuity equation method), and explain why the

conservative scheme is superior to the conventional δf scheme theoretically.

Applying the Fourier transform: $\partial/\partial t = -i\omega t$, $\mathbf{b_0} \cdot \nabla = ik_{\parallel}$ to the linear version of Eq. (5), we can derive the perturbed electron distribution in the uniform plasmas

$$\delta f = \frac{k_{\parallel} v_{\parallel}}{\omega - k_{\parallel} v_{\parallel}} \left(\phi - \frac{v_{\parallel}}{c} \delta A_{\parallel} \right) \frac{q_e}{T_{e0}} f_0, \qquad (14)$$

where $v_{\parallel} = p_{\parallel}/m_e$. Electron $E \times B$ drift cancels with ion species and does not appear.

The perturbed density and canonical flow can be derived by integrating Eq. (14) as

$$\delta n = \frac{en_{e0}}{T_{e0}} \left(\phi - \frac{1}{c} \frac{\omega}{k_{\parallel}} \delta A_{\parallel} \right) [1 + \xi_e Z(\xi_e)] \qquad (15)$$

and

$$U_{\parallel c} = \left\{ -\frac{e}{cm_e} \delta A_{\parallel} + \frac{e}{T_{e0}} \frac{\omega}{k_{\parallel}} \left(\phi - \frac{1}{c} \frac{\omega}{k_{\parallel}} \delta A_{\parallel} \right) [1 + \xi_e Z(\xi_e)] \right\}. \qquad (16)$$

In the conventional δf scheme, both electron density and canonical flow perturbations are calculated from the kinetic markers, thus we multiply the exact solutions Eqs. (15) and (16) by error coefficients to represent the values measured from the simulation with particle noise. The perturbed density and canonical flow calculated from kinetic markers with the particle noise effect can be expressed as[32]

$$\delta \tilde{n} = \frac{en_{e0}}{T_{e0}} \left(\phi - \frac{1}{c} \frac{\omega}{k_{\parallel}} \delta A_{\parallel} \right) [1 + \xi_e Z(\xi_e)](1 + \varepsilon_n) \qquad (17)$$

and

$$\tilde{U}_{\parallel c} = \left\{ -\frac{e}{cm_e} \delta A_{\parallel} + \frac{e}{T_{e0}} \frac{\omega}{k_{\parallel}} \left(\phi - \frac{1}{c} \frac{\omega}{k_{\parallel}} \delta A_{\parallel} \right) [1 + \xi_e Z(\xi_e)] \right\} \\ \times (1 + \varepsilon_u), \qquad (18)$$

where ε_n and ε_u represent the particle noise errors induced from the kinetic markers to the perturbed density and the perturbed canonical flow, respectively, Eqs. (17) and (18) become the exact solutions when $\varepsilon_n = \varepsilon_u = 0$.

Applying the Fourier transform $\nabla = i\mathbf{k}_{\perp}$ to Eqs. (7) and (11) and considering Eqs. (17) and (18), we can derive the dispersion relation of the shear Alfvén wave with particle noise error

$$\left(\frac{\omega^2}{k_{\parallel}^2 V_A^2} - 1 \right) [1 + \xi_e Z(\xi_e)]$$

$$= k_{\perp}^2 \rho_s^2 \frac{1}{1 + \varepsilon_u} - \frac{\beta_e}{2} \frac{m_i}{m_e} \frac{\varepsilon_u}{1 + \varepsilon_u} - \frac{1}{k_{\perp}^2 d_e^2} [1 + \xi_e Z(\xi_e)]$$

$$\times \frac{\varepsilon_u (1 + \varepsilon_n)}{1 + \varepsilon_u} + [1 + \xi_e Z(\xi_e)] \frac{\varepsilon_n - \varepsilon_u}{1 + \varepsilon_u}. \qquad (19)$$

Then, we can expand Eq. (19) using $|\varepsilon_n| \ll 1$ and $|\varepsilon_u| \ll 1$ and only keep the first order error terms

$$\left(\frac{\omega^2}{k_{\parallel}^2 V_A^2} - 1 \right) [1 + \xi_e Z(\xi_e)]$$

$$= k_{\perp}^2 \rho_s^2 (1 - \varepsilon_u) - \frac{\beta_e}{2} \frac{m_i}{m_e} \varepsilon_u - \frac{1}{k_{\perp}^2 d_e^2} [1 + \xi_e Z(\xi_e)] \varepsilon_u$$

$$+ [1 + \xi_e Z(\xi_e)](\varepsilon_n - \varepsilon_u). \qquad (20)$$

From Eq. (20), it is seen that the particle noise error is amplified with increasing β_e and the perpendicular wavelength through the second and third terms on the RHS, respectively, which explains the numerical difficulty of the electromagnetic simulation of the long wavelength modes with $k_{\perp}^2 d_e^2 \ll 1$ in high β_e plasmas. For example, the numerically high frequency modes dominate in the simulation of long wavelength ($k_{\perp}^2 d_e^2 \ll 1$) shear Alfvén waves by using the conventional δf scheme as shown by Fig. 3, which are caused by the third error term on the RHS of Eq. (20).

In the conservative scheme, we use the kinetic markers to calculate the perturbed canonical flow as Eq. (18). The parallel vector potential with the error effect can be calculated by using Eqs. (7) and (18)

$$\delta A_{\parallel} = \frac{c \frac{\omega}{k_{\parallel}} [1 + \xi_e Z(\xi_e)](1 + \varepsilon_u)}{-c^2 k_{\perp}^2 \lambda_D^2 + v_{the}^2 \varepsilon_u + \frac{\omega^2}{k_{\parallel}^2} [1 + \xi_e Z(\xi_e)](1 + \varepsilon_u)} \phi. \qquad (21)$$

From Eqs. (9), (10), and (21), the perturbed density with particle noise error in the linear and uniform plasmas is

$$\delta n = \frac{-\frac{c^2 k_{\perp}^2}{4\pi e} [1 + \xi_e Z(\xi_e)](1 + \varepsilon_u)}{-c^2 k_{\perp}^2 \lambda_D^2 + v_{the}^2 \varepsilon_u + \frac{\omega^2}{k_{\parallel}^2} [1 + \xi_e Z(\xi_e)](1 + \varepsilon_u)} \phi. \qquad (22)$$

From Eqs. (11) and (22), the dispersion relation of the shear Alfvén wave with particle noise error in the conservative scheme is

$$\left(\frac{\omega^2}{k_{\parallel}^2 V_A^2} - 1 \right) [1 + \xi_e Z(\xi_e)] = k_{\perp}^2 \rho_s^2 \frac{1}{1 + \varepsilon_u} - \frac{\beta_e}{2} \frac{m_i}{m_e} \frac{\varepsilon_u}{1 + \varepsilon_u}. \qquad (23)$$

Keeping the first order terms with respect to particle noise error, Eq. (23) can be written as

$$\left(\frac{\omega^2}{k_{\parallel}^2 V_A^2} - 1 \right) [1 + \xi_e Z(\xi_e)] = k_{\perp}^2 \rho_s^2 (1 - \varepsilon_u) - \frac{\beta_e}{2} \frac{m_i}{m_e} \varepsilon_u. \qquad (24)$$

Compared to Eq. (20), there is no particle noise error term related to the perpendicular wavelength in Eq. (24). It is because that the continuity equation guarantees the consistency between ε_n and ε_u in the conservative scheme, and the last two terms on the RHS of Eq. (19) cancel with each other. Thus, the conservative scheme is more robust than the conventional δf scheme for the simulations of long wavelength electromagnetic modes. For example, the conservative scheme can simulate shear Alfvén waves in the long

wavelength regimes accurately, while the conventional δf scheme fails as shown by Fig. 3. From Eqs. (20) and (24), it is also noticed that finite β_e can amplify error terms for both schemes. However, we can simulate the shear Alfvén waves with sufficient accuracy in the very high β_e regime by using the conservative scheme as shown by Fig. 5, which indicates that finite β_e effects are not as severe as long wavelength ($k_\perp^2 d_e^2 \approx 0$) effects on the numerical properties of electromagnetic simulations.

B. Error effects on the parallel electric field $\delta E_\parallel$

As we have illustrated before, the perturbed density and canonical flow calculated from the kinetic markers do not satisfy the electron continuity equation, which leads to the inconsistency of the corresponding electrostatic potential and vector potential in the conventional perturbative (δf) simulation. However, the parallel electric field $\delta E_\parallel \approx 0$ in the long wavelength (ideal MHD) limit, which requires that the electrostatic electric field $\delta E_\parallel^e = -\mathbf{b_0} \cdot \nabla \phi$ and the inductive electric field $\delta E_\parallel^i = (1/c)\partial \delta A_\parallel / \partial t$ evolve consistently and their major parts can cancel with each other in the simulation. Thus, any inconsistency of $\delta E_\parallel^e$ and $\delta E_\parallel^i$ can lead to the unphysically large $\delta E_\parallel$, and cause the numerical instability in the conventional perturbative (δf) scheme. In this part, the error effects on the parallel electric field $\delta E_\parallel$ are discussed for both the conventional δf scheme and conservative scheme.

In the conventional δf scheme, applying the Fourier transform $\nabla = i\mathbf{k}_\perp$ to Eqs. (7) and (11), and considering Eqs. (17) and (18), the electrostatic potential and vector potential can be represented as

$$\phi = -\frac{4\pi e n_{e0} V_A^2}{c^2 k_\perp^2}\frac{k_\parallel}{\omega}\left(\frac{1+\varepsilon_n}{1+\varepsilon_u} - \frac{1+\varepsilon_n}{1+k_\perp^2 d_e^2}\right)\tilde{U}_{\parallel c}, \quad (25)$$

$$\delta A_\parallel = -\frac{d_e^2}{1+k_\perp^2 d_e^2}\frac{4\pi e n_{e0}}{c}\tilde{U}_{\parallel c}. \quad (26)$$

Thus, the parallel electric field $\delta E_\parallel$ in the conventional δf scheme is

$$\delta E_\parallel = i\frac{m_e}{e\omega}\frac{k_\parallel^2 V_A^2}{1+k_\perp^2 d_e^2}\left(\frac{\omega^2}{k_\parallel^2 V_A^2} - 1\right)\tilde{U}_{\parallel c}$$
$$+ i\frac{m_e}{e\omega}\frac{k_\parallel^2 V_A^2}{k_\perp^2 d_e^2}\left(\frac{1+\varepsilon_n + k_\perp^2 d_e^2}{1+k_\perp^2 d_e^2} - \frac{1+\varepsilon_n}{1+\varepsilon_u}\right)\tilde{U}_{\parallel c}. \quad (27)$$

By keeping the first order error terms based on $|\varepsilon_n| \ll 1$ and $|\varepsilon_u| \ll 1$, Eq. (27) can be simplified as

$$\delta E_\parallel = i\frac{m_e}{e\omega}\frac{k_\parallel^2 V_A^2}{1+k_\perp^2 d_e^2}\left(\frac{\omega^2}{k_\parallel^2 V_A^2} - 1\right)\tilde{U}_{\parallel c}$$
$$+ i\frac{m_e}{e\omega}\frac{k_\parallel^2 V_A^2}{k_\perp^2 d_e^2}\left(\varepsilon_u - \varepsilon_n \frac{k_\perp^2 d_e^2}{1+k_\perp^2 d_e^2}\right)\tilde{U}_{\parallel c}. \quad (28)$$

The last term on the RHS of Eq. (28) is due to inconsistency between ε_n and ε_u, which will be amplified when $k_\perp^2 d_e^2$ is small.

In the conservative scheme, the perturbed density is calculated from Eq. (9) instead of Eq. (17). The electrostatic potential can be derived by using Eqs. (9)–(11) and (26) as

$$\phi = -\frac{4\pi e n_{e0} V_A^2}{c^2 k_\perp^2}\frac{k_\parallel}{\omega}\left(\frac{k_\perp^2 d_e^2}{1+k_\perp^2 d_e^2}\right)\tilde{U}_{\parallel c}. \quad (29)$$

By using Eqs. (26) and (29), the parallel electric field $\delta E_\parallel$ in the conservative scheme is

$$\delta E_\parallel = i\frac{m_e}{e\omega}\frac{k_\parallel^2 V_A^2}{1+k_\perp^2 d_e^2}\left(\frac{\omega^2}{k_\parallel^2 V_A^2} - 1\right)\tilde{U}_{\parallel c}. \quad (30)$$

Comparing Eqs. (28) and (30) in the long wavelength limit with $k_\perp^2 d_e^2 \ll 1$, it is seen that $\delta E_\parallel \approx 0$ with $\omega^2 \approx k_\parallel^2 V_A^2$ for the conservative scheme, while $\delta E_\parallel \propto 1/k_\perp^2 d_e^2$ with $\omega^2 \approx k_\parallel^2 V_A^2$ for the conventional δf scheme due to the inconsistency between the perturbed density and canonical flow. Thus, the conservative scheme can guarantee $\delta E_\parallel \approx 0$ in the simulation as shown by Fig. 4(a), while the conventional δf scheme causes the unphysically large amplitude of $\delta E_\parallel$ in the simulation as shown by Fig. 4(b), which is due to the last error term on the RHS of Eq. (28).

V. CONCLUSIONS

In this work, we present an innovative conservative scheme to solve the numerical difficulty of the electromagnetic gyrokinetic particle simulation with kinetic electrons. In the conventionally electromagnetic perturbative (δf) simulation with drift kinetic electrons of $p_\parallel$ formulation, we found that perturbed density and perturbed canonical flow, calculated from the kinetic markers, do not satisfy the continuity equation due to the particle noise, which causes the inconsistency between the electrostatic potential and parallel vector potential and leads to an unphysically large parallel electric field in the long wavelength MHD regime. In the conservative scheme, we use the electron continuity equation to time advance the electron density perturbation using the perturbed mechanical flow calculated from the parallel vector potential, and the parallel vector potential is solved by using the canonical flow from the kinetic markers, which guarantees the consistency between electrostatic and parallel vector potentials. Furthermore, the conservative scheme helps to relax the perpendicular grid size without resolving the electron skin depth when the wavelength is longer than the electron skin depth. However, in the conventional electromagnetic δf scheme, the perpendicular grid size needs to resolve the electron skin depth even for the long wavelength MHD wave simulation. The simulations of the shear Alfvén wave dispersion relation and continuum damping are well benchmarked with the theory by using the conservative scheme. In the conservative scheme, simulation of the long wavelength shear Alfvén wave, the electrostatic component, and the inductive component of the electric field cancel with each other as expected. Finally, comparison of Alfvén wave propagation results between gyrokinetic particle simulation and fluid simulation shows that gyrokinetic particle simulation is superior to the fluid simulation by physically avoiding

the singular mode structures through electron Landau damping. Building on the linear application of the conservative scheme to shear Alfvén wave simulation, the nonlinear simulation results will be reported in the future work. Meanwhile, the application of the conservative scheme on the drift kinetic electron model with $v_{\parallel}$ formulation combining with the split weight scheme has been reported in another work.[33]

[1] J. F. Drake, N. T. Gladd, C. S. Liu, and C. L. Chang, Phys. Rev. Lett. **44**, 994 (1980).
[2] Z. Wang, Z. Lin, I. Holod, W. W. Heidbrink, B. Tobias, M. V. Zeeland, and M. E. Austin, Phys. Rev. Lett. **111**, 145003 (2013).
[3] J. V. W. Reynders, Ph.D thesis, Princeton University, 1992.
[4] J. C. Cummings, Ph.D. thesis, Princeton University, 1995.
[5] I. Holod and Z. Lin, Phys. Plasmas **20**, 032309 (2013).
[6] Z. Lin, paper presented at SciDAC Microturbulence Project Meeting, General Atomics (2001).
[7] J. Candy and R. E. Waltz, J. Comput. Phys. **186**, 545–581 (2003).
[8] Y. Chen and S. E. Parker, J. Comput. Phys. **189**, 463–475 (2003).
[9] W. W. Lee, J. L. V. Lewandowski, T. S. Hahm, and Z. Lin, Phys. Plasmas **8**, 4435 (2001).
[10] Z. Lin and L. Chen, Phys. Plasmas **8**, 1447 (2001).
[11] R. Hatzky, A. Konies, and A. Mishchenko, J. Comput. Phys. **225**, 568–590 (2007).
[12] I. Holod, W. L. Zhang, Y. Xiao, and Z. Lin, Phys. Plasmas **16**, 122307 (2009).
[13] Y. Chen and S. E. Parker, Phys. Plasmas **18**, 055703 (2011).
[14] E. A. Startsev and W. W. Lee, Phys. Plasmas **21**, 022505 (2014).
[15] A. Mishchenko, M. Cole, R. Kleiber, and A. Könies, Phys. Plasmas **21**, 052113 (2014).
[16] J. Bao, Z. Lin, A. Kuley, and Z. X. Wang, Phys. Plasmas **23**, 062501 (2016).
[17] J. Bao, Z. Lin, A. Kuley, and Z. X. Wang, Nucl. Fusion **56**, 066007 (2016).
[18] T. S. Hahm, W. W. Lee, and A. Brizard, Phys. Fluids **31**, 1940 (1988).
[19] A. J. Brizard and T. S. Hahm, Rev. Mod. Phys. **79**(2), 421 (2007).
[20] A. M. Dimits and W. W. Lee, J. Comput. Phys. **107**, 309 (1993).
[21] S. E. Parker and W. W. Lee, Phys. Fluids B **5**, 77 (1993).
[22] W. Deng, Z. Lin, and I. Holod, Nucl. Fusion **52**, 023005 (2012).
[23] W. W. Lee, J. Comput. Phys. **72**, 243 (1987).
[24] Z. Lin, T. S. Hahm, W. W. Lee, W. M. Tang, and R. B. White, Science **281**, 1835 (1998).
[25] D. Liu and L. Chen, Phys. Scr. **84**, 025506 (2011).
[26] D. Liu, J. Bao, T. Han, J. Wang, and Z. Lin, Phys. Plasmas **23**, 022502 (2016).
[27] H. Grad, Phys. Today **22**(12), 34 (1969).
[28] J. Tataronis and W. Grossmann, Z. Phys. **261**, 203 (1973).
[29] W. Grossmann and J. Tataronis, Z. Phys. **261**, 217 (1973).
[30] A. Hasegawa and C. Uberoi, *The Alfvén Wave* (U.S. Department of Energy Technical Information Center, Oak Ridge, DOE/TIC-11191, 1982), Vol. 46, p. 54.
[31] A. Hasegawa and L. Chen, Phys. Fluids **19**, 1924 (1976).
[32] E. Startsev, W. W. Lee, and W. Wang, Bull. Am. Phys. Soc. **60**, JP12.129 (2015).
[33] J. Bao, Z. Lin, and Z. X. Lu, Phys. Plasmas **24**, 102516 (2017).